https://doi.org/10.3311/PPee.39553

Periodica Polytechnica Electrical Engineering and Computer Science, 69(4), pp. 357–371, 2025

A Probabilistic Assessment Method of Voltage Deviation Risk for Wind Power Access to Distribution Network Based on Total Probability Formula and Nataf Transformation

Ruohui Mo[1*], Yongqi He[1], Jun Wang[1], Minglong Zou[1], Jialin Song[1]

[1] Electric Power Dispatch and Control Center, Hainan Power Grid Co., Ltd., Hairuihou Road 23, 570100 Haikou, Hainan, China
[*] Corresponding author, e-mail: morh@hn.csg.cn

Received: 12 December 2024, Accepted: 06 October 2025, Published online: 13 November 2025

Abstract

Driven by the "dual-carbon" goals, the large-scale integration of wind power into distribution networks poses challenges to voltage stability due to its inherent volatility and uncertainty. To address it, this paper proposes a probabilistic assessment method based on the total probability formula that incorporates wind speed correlation to effectively evaluate voltage deviation. Firstly, the probability model of wind power is established according to the uncertainty of wind speed considering the correlation. Secondly, the wind power output is discretized and aggregated to ensure that the resulting random variables in the combined state approximately follow a normal distribution. Spatial correlations in wind speed are accounted for using the Nataf transformation. Furthermore, the probability of each aggregated wind power state determines its weight. These weights are then used to accumulate and integrate the probabilistic power flow (PPF) results. The total PPF calculation accounts for wind power uncertainty, following the Total Probability Formula (TPF) framework. Finally, considering the indexes with the probability and severity of voltage deviation, the comprehensive risk indicator for voltage exceeding limits is constructed. Based on the IEEE-33 bus test system, the proposed TPF method is compared with Monte Carlo Simulation (MCS) and the Two-Point Estimation Method (2PEM). The comparison demonstrates its superior computational accuracy and efficiency, establishing it as an effective tool for assessing the impact of wind power integration on distribution networks.

Keywords

probabilistic assessment, probabilistic power flow, correlation, voltage risk, distribution network

1 Introduction

1.1 Background

Under the promotion of the "dual-carbon" strategic objectives, distributed and centralized wind power generation, as crucial components of clean energy, play significant roles in constructing new power systems [1]. By the end of 2024, China's installed wind power capacity reached approximately 510 million kilowatts, with photovoltaic capacity around 840 million kilowatts, maintaining a utilization rate above 95% [2]. The increasing integration of wind power into distribution networks, particularly under the "Thousand Townships and Ten Thousand Villages Wind Utilization Initiative", has rendered the interaction between distributed wind power and distribution networks increasingly complex [3]. During wind turbine operation, wind speed fluctuations are transformed into power variations through a cubic relationship, thereby inducing voltage fluctuations. Influenced by multiple factors including wind speed and meteorological conditions, wind power exhibits marked uncertainty [4, 5]. When wind power output exceeds local load demand, it alters the voltage distribution and power flow direction in distribution networks [6]. This phenomenon not only expands the voltage fluctuation range but also triggers voltage quality issues such as voltage deviation exceedance [7]. Therefore, voltage risk assessment for wind-integrated distribution networks constitutes a critical link in ensuring secure and stable system operation.

1.2 Literature review

Traditional methods for voltage risk analysis and assessment in distribution networks include sensitivity analysis [8], continuation power flow method [9], and modal analysis [10]. These deterministic approaches, based on fixed operational scenarios, offer advantages such as computational simplicity, high efficiency, and intuitive

Cite this article as: Mo, R., He, Y., Wang, J., Zou, M., Song, J. "A Probabilistic Assessment Method of Voltage Deviation Risk for Wind Power Access to Distribution Network Based on Total Probability Formula and Nataf Transformation", Periodica Polytechnica Electrical Engineering and Computer Science, 69(4), pp. 357–371, 2025. https://doi.org/10.3311/PPee.39553

results, enabling the evaluation of system security margins [11, 12]. However, wind power output exhibits inherent uncertainty and randomness, with operational scenarios being non-unique. The extreme scenario assumptions in deterministic methods may lead to assessment results deviating from actual operating conditions [13]. Notably, adjacent wind turbines demonstrate significant spatial correlations in wind speed exposure and power generation [14]. Neglecting such spatial correlations could severely compromise the accuracy of voltage risk assessments [15]. For voltage quality analysis in wind-integrated distribution networks considering uncertainty, probabilistic risk assessment based on probabilistic power flow (PPF) calculation proves effective. Common PPF computation methods fall into three categories [16]: Monte Carlo Simulation (MCS), analytical approaches, and approximation methods [17]. While MCS achieves the highest accuracy, it requires extensive random sampling and iterative computations, resulting in low efficiency [18]. Analytical approaches generate significant errors when input variables exhibit large fluctuations, whereas approximation methods face scalability limitations due to constrained sampling sizes [19].

Singh et al. [20] proposed a Cornish-Fisher expansion-based risk assessment method for distribution networks. However, in wind-integrated distribution networks, non-Gaussian distributions of input variables may induce computational deviations, and the spatial correlations among wind turbines remain unaddressed. Table 1 shows a comparison between existing research and the current study. Ma et al. [21] employed multi-order semi-invariants combined with Gram-Charlier series expansion for probabilistic static voltage stability assessment in wind-integrated systems. Nevertheless, its limited capability to model non-Gaussian distributions introduces significant errors in voltage risk evaluation. Yu et al. [22] developed a time-segmented Monte Carlo sampling method to assess voltage risks from distributed wind and photovoltaic integration, addressing their intermittency. However, this approach suffers from high computational costs and inefficiency. Nejadfard-jahromi et al. [23] introduced a preventive control-based method for rapid voltage stability margin evaluation in distribution networks with electric vehicles and wind power, yet the exclusion of wind power correlations compromises assessment completeness. Canudo et al. [24] proposed an improved point estimate method incorporating local voltage stability indices, but its neglect of wind farm spatial correlations leads to non-negligible errors in system voltage stability assessment. In contrast, the Total Probability Formula (TPF) inherently avoids distribution-fitting assumptions (e.g., normality deviations) while strictly adhering to the probability conservation principle (summing to unity) [25]. By integrating probabilistic distributions from PPF calculations, TPF demonstrates superior computational accuracy for voltage risk quantification.

1.3 Contribution

In light of these considerations, this paper innovatively integrates wind speed spatial correlations with the TPF to propose a voltage deviation risk assessment framework for wind-integrated distribution networks. The framework combines TPF and Nataf transformation-based PPF calculations, establishing a spatially correlated wind speed probability model. By leveraging voltage deviation probabilities and severity indices, it constructs a comprehensive risk assessment framework to quantitatively evaluate the impact of wind speed correlations on voltage deviation risks. The key contributions are summarized as follows:

1. A data-driven wind speed parameter modeling method incorporating spatial correlations is developed to accurately characterize the operational uncertainty of wind turbines.

Table 1 Comparison between existing research and this study

Research direction	Research contents	Research methods	Methods of this paper
Probabilistic Power Flow (PPF) calculation methods	Probability power flow result distribution considering the randomness of wind power (voltage, power, etc.) [20].	Analysis methods (such as convolution) [9], Monte Carlo simulation [17], approximation methods (such as Cornish Fisher expansion) [19].	The proposed PPF method, based on TPF combined with the Nataf transformation, efficiently computes PPF in distribution networks with correlated wind power. This approach improves computational accuracy while maintaining low computational costs.
Voltage deviation risk assessment	Statistical evaluation of the probability of bus voltage exceeding the limit [14], standard deviation and average value of voltage amplitude [15].	Probability density function fitting [11], risk indicators [12].	Based on the PPF method combining TPF and Nataf transformation, the comprehensive risk index is formed by considering the probability and severity of voltage deviation. The comprehensive risk of voltage deviation has been evaluated. Comprehensively reflect the impact of wind power on the distribution network.

2. A piecewise linearization technique is introduced to discretize wind power outputs, coupled with a PPF computation method based on TPF and Nataf transformation, significantly enhancing computational efficiency.
3. A composite voltage risk index integrating deviation probability and severity is formulated, establishing a TPF-based PPF framework for voltage deviation risk assessment to improve result accuracy.
4. The proposed TPF-Nataf probabilistic risk assessment method provides practical case studies and analytical tools for evaluating the grid integration impacts of the "Thousand Townships and Ten Thousand Villages Wind Utilization Initiative".

The rest of this paper is organized as follows:
- Section 2 introduces the wind speed probability model and the correlation characterization of random variables.
- In Section 3 introduces the PPF calculation method based on TPF and proposes a comprehensive voltage risk method and calculation evaluation process.
- Section 4 verifies the framework through case analysis and discussion.
- Finally, Section 5 is the conclusion.

2 Probability model and correlation of input random variables

2.1 Probabilistic modeling of wind power

Due to the deterministic models not reflecting the randomness and volatility of wind power [26], the commonly utilized Weibull distribution is used to describe the probability model of wind speed, as shown in Eq. (1). Equation (2) represents the cumulative distribution function (CDF) of wind speed [27]. The relationship between the active power output of wind turbines and wind speed can be expressed as a piecewise function in Eq. (3).

$$f(v)=\frac{k}{\lambda}\left(\frac{v}{\lambda}\right)^{k-1}e^{-(v/\lambda)^k} \tag{1}$$

$$F(v)=1-e^{-(v/\lambda)^k} \tag{2}$$

$$P_{DG}=\begin{cases}0, & 0\le v\le v_1 \text{ or } v\ge v_3\\ P_{DG,w}\dfrac{v-v_1}{v_2-v_1}, & v_1<v<v_2\\ P_{DG,w}, & v_2\le v<v_3\end{cases} \tag{3}$$

Where v is the wind speed; λ and k are respectively the scale parameter and shape parameter of the Weibull distribution; $f(\cdot)$ is the probability density function (PDF); v_1, v_2 and v_3 are the cut-in wind speed, rated wind speed, and cut-out wind speed, respectively; P_{DG} and $P_{DG,w}$ are respectively represent the actual output and rated output of the wind turbines.

For doubly-fed induction generators (DFIGs), optimization algorithms are employed to enhance operational performance [28–30]. Under the constant power factor control strategy, the proportional relationship between active power P_s and reactive power Q_s at the stator side follows Eq. (4) [31].

$$Q_s=P_s\tan(\varphi) \tag{4}$$

In Eq. (4), φ is the power factor angle. Ignoring the reactive power on the rotor side, the reactive power $Q_{G,w}$ generated by the wind turbine is approximately equal to the reactive power on the stator side.

2.2 Probability model of load

The random fluctuation of electric load is dependent on the cyclical or regular changes in social production and life. As a result, the random variation of electric load can be described as the Normal distribution characteristics [19]. The PDF of active and reactive power of electrical loads can be described as follows:

$$f(P)=\frac{1}{\sqrt{2\pi}\sigma_p}e^{-(P-\mu_p)^2/2\sigma_p^2} \tag{5}$$

$$f(Q)=\frac{1}{\sqrt{2\pi}\sigma_q}e^{-(Q-\mu_q)^2/2\sigma_q^2}, \tag{6}$$

where $f(\cdot)$ is the PDF of the electric load; P and Q respectively represent active and reactive power; μ_p and μ_q respectively denote the average of active and reactive power of electric bus load; σ_p and σ_q are respectively the standard deviation of active and reactive power of electric bus load.

2.3 Correlation of wind power output

The Pearson correlation coefficient is a statistical measure that can be used to assess the linear relationship between two random variables [32]. This correlation index is easy to calculate and requires little data. The Pearson correlation coefficient better captures the true relationship between two variables. Let the n-dimensional random variables $\boldsymbol{X}(x_1, x_2, x_i, \ldots, x_n)$ and $\boldsymbol{Y}(y_1, y_2, y_i, \ldots, y_n)$, $(i, j = 1, 2, \ldots, n)$. In mathematics, the Pearson correlation coefficient between two random variables $\boldsymbol{X}$ and $\boldsymbol{Y}$ is given by Eq. (7) [5]:

$$\rho(\boldsymbol{X},\boldsymbol{Y})=\frac{Cov(\boldsymbol{X},\boldsymbol{Y})}{\sqrt{E_X\cdot E_Y}}=\frac{\sum_{i=1}^{n}(x_i-\bar{x})(y_i-\bar{y})}{\sqrt{\sum_{i=1}^{n}(x_i-\bar{x})^2\cdot(y_i-\bar{y})^2}}, \quad (7)$$

where $\bar{x}$ and $\bar{y}$ are respectively the average values of $\boldsymbol{X}$ and $\boldsymbol{Y}$. E_X and E_Y are respectively the variances of $\boldsymbol{X}$ and $\boldsymbol{Y}$. The correlation coefficient $\rho(\boldsymbol{X}, \boldsymbol{Y})$ is in [−1, 1]. where −1 indicates a completely negative linear relationship, 1 indicates a completely positive linear relationship, and 0 indicates no linear relationship.

2.4 Correlation processing based on Nataf transform

The Nataf transformation converts arbitrary random variables into standard normal variables for probability analysis and risk assessment. In addition, the calculation accuracy of the Nataf transform is high [33].

The n-dimensional random variable $\boldsymbol{Z}(z_1, z_2, z_i, \ldots, z_n)$ distributed a standard Normal is introduced. The correlation coefficient between z_i and z_j is ρ_{Zij} (i, j = 1, 2, …, n). According to the principle of equal probability, x_i and z_j satisfy:

$$z_i=\Phi^{-1}\left(F_i(x_i)\right) \quad i=1,2,\ldots,n, \quad (8)$$

where $\Phi^{-1}(\cdot)$ is the inverse of the CDF of the standard Normal distribution; $F_i(\cdot)$ is the CDF of the random variable x_i.

According to Eq. (8) and the definition of the correlation coefficient, the relationship between ρ_{Xij} and ρ_{Zij} is

$$\rho_{Xij}=\frac{\int_{-\infty}^{\infty}\int_{-\infty}^{\infty}F_i^{-1}\left(\Phi(z_i)\right)F_j^{-1}\left(\Phi(z_j)\right)\varphi_{zij}(z_i,z_j)\mathrm{d}z_i\mathrm{d}z_j-\mu_i\mu_j}{\sigma_i\sigma_j}, \quad (9)$$

where μ and σ are respectively the average and standard deviation of x; φ_{zij} is the PDF of the standard binary Normal distribution; the correlation coefficient of φ_{zij} is ρ_{Zij}.

According to Eq. (9), the correlation coefficient matrix $\boldsymbol{C}_Z$ of $\boldsymbol{Z}(z_1, z_2, z_i, \ldots, z_n)$ can be obtained. The Cholesky decomposition $\boldsymbol{C}_Z$ can be obtained [34]:

$$\boldsymbol{C}_Z=\boldsymbol{L}\boldsymbol{L}^T. \quad (10)$$

With the lower triangular matrix $\boldsymbol{L}$ of the Cholesky decomposition, the correlated $\boldsymbol{Z}(z_1, z_2, z_i, \ldots, z_n)$ can be converted to an independent standard normally distributed random variable $\boldsymbol{Y}(y_1, y_2, y_i, \ldots, y_n)$, i.e.,

$$\boldsymbol{Y}=\boldsymbol{L}^{-1}\boldsymbol{Z}. \quad (11)$$

Therefore, the correlation of wind speed can be processed by Nataf transformation.

3 PPF calculation and voltage deviation risk assessment method based on TPF

The PPF calculation method based on TPF considering wind speed correlation is proposed to address the uncertainty of wind power distribution network operation. The piecewise linearization technique is introduced to discretize the output power of wind turbines. Since only the influence of input variable uncertainty is considered, the expansion of Gram Charlier series with high-order moments omitted can be adopted.

3.1 Power flow calculation model

The bus power equation of the power system is as follows [35]:

$$\begin{aligned}P_i&=V_i\sum_{j=1}^{n}V_j\left(G_{ij}\cos\theta_{ij}+B_{ij}\sin\theta_{ij}\right)\\ Q_i&=V_i\sum_{j=1}^{n}V_j\left(G_{ij}\sin\theta_{ij}-B_{ij}\cos\theta_{ij}\right),\end{aligned} \quad (12)$$

where P_i and Q_i are respectively the injection amounts of active and reactive power of bus i; V_i and θ_i are respectively the voltage amplitude and its angle of bus i; G_{ij} and B_{ij} are respectively the real and imaginary parts of admittance matrix elements.

Equation (12) can be simplified as follows [36]:

$$\begin{cases}\boldsymbol{W}=f(\boldsymbol{H})\\ \boldsymbol{K}=L(\boldsymbol{H})\end{cases}, \quad (13)$$

where $\boldsymbol{W}$ is the matrix composed of the injected power for each bus; $\boldsymbol{H}$ is the state matrix of each bus; $\boldsymbol{K}$ is the matrix of branch power flow; $f(\boldsymbol{H})$ and $L(\boldsymbol{H})$ are respectively the bus voltage equation and branch power flow equation.

The injected bus power $\boldsymbol{W}$ is regarded as the input random variable of the grid, then the results $\boldsymbol{H}$ and $\boldsymbol{K}$ of power flow calculation can be regarded as the output random variables. The above three random variables can be written as the form of reference value with random disturbance value, that is

$$\begin{cases} \boldsymbol{W} = \boldsymbol{W}_0 + \Delta \boldsymbol{W} \\ \boldsymbol{H} = \boldsymbol{H}_0 + \Delta \boldsymbol{H} \\ \boldsymbol{K} = \boldsymbol{K}_0 + \Delta \boldsymbol{K} \end{cases}, \tag{14}$$

where $\boldsymbol{W}_0$, $\boldsymbol{H}_0$ and $\boldsymbol{K}_0$ are respectively the reference values or expectation values of bus injection power, bus state and branch power flow; $\Delta\boldsymbol{W}$, $\Delta\boldsymbol{H}$ and $\Delta\boldsymbol{K}$ are respectively the random disturbance values of bus injection power, bus state and branch power flow.

The power flow equations at the reference operating point are expanded using the Taylor series. Neglecting the higher-order terms, the linearized expression of the power flow equation can be shown as follows:

$$\begin{cases} \Delta \boldsymbol{W} = \boldsymbol{J}_0 \Delta \boldsymbol{H} \\ \Delta \boldsymbol{K} = \boldsymbol{D}_0 \Delta \boldsymbol{H} \end{cases} \tag{15}$$

$$\begin{cases} \Delta \boldsymbol{H} = \boldsymbol{J}_0^{-1} \Delta \boldsymbol{W} = \boldsymbol{S}_0 \Delta \boldsymbol{W} \\ \Delta \boldsymbol{K} = \boldsymbol{D}_0 \boldsymbol{J}_0^{-1} \Delta \boldsymbol{W} = \boldsymbol{T}_0 \Delta \boldsymbol{W} \end{cases}, \tag{16}$$

where $\boldsymbol{J}_0$ is the Jacobian matrix used in the last iteration of power flow calculation; $\boldsymbol{D}_0$ is a matrix of order $2b \times 2n$, in which b is the number of branches and n is the number of buses; $\boldsymbol{D}_0 = \dfrac{\partial \boldsymbol{K}}{\partial \boldsymbol{H}}\Big|_{\boldsymbol{H}=\boldsymbol{H}_0}$; $\boldsymbol{S}_0 = \boldsymbol{J}_0^{-1}$; $\boldsymbol{T}_0 = \boldsymbol{D}_0 \boldsymbol{J}_0^{-1}$ is the sensitivity matrix.

3.2 Discretization of a stochastic model of wind power generation

In Eq. (3), when the wind speed satisfies the condition $v \in [v_1, v_2]$, the output power approximated as a linear state of the wind turbines in this interval of wind speed $[v_1, v_2]$ can be divided into m segments according to the set power step size for discretization [37]. The relationship between wind power and wind speed is shown in Fig. 1. Taking the i^{th} paragraph on wind speed as an example, the power of wind turbines is approximately $(P_i + P_{i+1})/2$ with a probability in Eq. (17). After the discretization process, $m + 2$ discrete values and their corresponding probabilities are used to describe the randomness of the output power for the wind turbine [37].

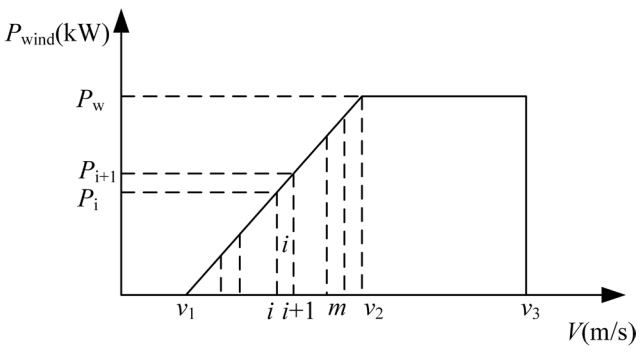

Fig. 1 Relationship between wind power and wind speed

$$P_{rob}\left[\left(P_i + P_{i+1}\right)/2\right] = F\left(v_{i+1}^m\right) - F\left(v_i^m\right) = e^{-\left(v_i^m/\lambda\right)^k} - e^{-\left(v_{i+1}^m/\lambda\right)^k},$$
$$v_1 < v < v_2 \tag{17}$$

Where v is the wind speed; λ and k are respectively the scale parameter and shape parameter; v_i^m is the i^{th} segment wind speed discretized by wind speed's interval $[v_1, v_2]$; $F(v)$ is the CDF of wind speed; $P_{rob}[(P_i + P_{i+1})/2]$ is the probability when the output power of wind turbine is in the i^{th} segment at $(P_i + P_{i+1})/2$.

Meanwhile, $P_{rob}(0)$ is the probability when the output power of the wind turbine is 0. $P_{rob}(P_w)$ is the probability when the output power of the wind turbine is P_w. The calculations of $P_{rob}(0)$ and $P_{rob}(P_w)$ are shown in Eq. (18) and Eq. (19), respectively.

$$P_{rob}\left(0\right) = F\left(v_1\right) + \left[1 - F\left(v_3\right)\right] = 1 - e^{-\left(v_1/\lambda\right)^k} + e^{-\left(v_3/\lambda\right)^k},$$
$$v < v_1 \text{ or } v > v_3 \tag{18}$$

$$P_{rob} = \left(P_w\right) = F\left(v_3\right) - F\left(v_2\right) = e^{-\left(v_2/\lambda\right)^k} - e^{-\left(v_3/\lambda\right)^k},$$
$$v_2 < v < v_3 \tag{19}$$

3.3 Combination of multiple discretization states of wind power

The output power of multiple wind turbines needs to be respectively discretized. Then, the output states of multiple wind turbines are combined to obtain N combinations of output power for the system's multiple wind turbines. N is the superposition of the discretized fragments m of wind power, as shown in Eq. (20). Furthermore, Eq. (21) represents the n^{th} output combination state, where $P_i(C_n)$ is the output power of the i^{th} wind turbine in the n^{th} state. The probability of the n^{th} state is shown in Eq. (22), where $P_{rob}[P_i(C_n)]$ is the probability when the output power of the n^{th} wind power station is $P_i(C_n)$.

$$N = \prod_{i=1}^{K} \left(m_i + 2\right) \tag{20}$$

$$C_n = \left\{P_1\left(C_n\right), P_2\left(C_n\right), \cdots P_i\left(C_n\right), \cdots P_K\left(C_n\right)\right\},\ n \in \left[1, N\right] \tag{21}$$

$$P_{rob}\left(C_n\right) = \prod_{i=1}^{K} P_{rob}\left[P_i\left(C_n\right)\right] \tag{22}$$

3.4 PPF results calculation based on TPF

Event A in the system is defined as a state variable x which is less than x_A. $F(x_A)$ indicates its cumulative distribution probability, and $f(x_A)$ represents its probability density. $P_{rob}(C_n)$ is denoted as $P_{rob}(B)$. The probability of an event A $P_{rob}(A)$ is shown in Eq. (23) by the TPF. When the wind power output is a constant value, for the conditional event $A|B_n$, the random variables in the system meet the Normal distribution. Therefore, the CDF of the conditional event $A|B_n$ is shown in Eq. (24) [38].

$$P_{rob}\left(A\right)=\sum_{n=1}^{N}P_{rob}\left(A\middle|B_n\right)\times P_{rob}\left(B_n\right) \tag{23}$$

$$F\left(x_A\middle|B_n\right)=\int_{-\infty}^{x_A}\frac{1}{\sigma_n\sqrt{2\pi}}e^{\frac{-(t-\mu_n)^2}{2\sigma_n^2}}\,\mathrm{d}t \tag{24}$$

With the discretized stochastic model for wind power output, there are N Gauss functions in the N output combination state of wind power generation for any system state variable to be sought. From Eq. (23), the probability $P_{rob}(B_n)$ of the corresponding power combination state can be accumulated one by one to obtain a complete PDF. In theory, when N approaches infinity, that is, when the step size approaches 0, the distribution function tends towards the true distribution, as shown in Eqs. (25) and (26). The above process is based on the direct derivation of the established discrete model of wind power generation.

$$F\left(x_A\right)=\sum_{n=1}^{N}\left\{P_{rob}\left(B_n\right)\int_{-\infty}^{x_A}\frac{1}{\sigma_n\sqrt{2\pi}}e^{\frac{-(t-\mu_n)^2}{2\sigma_n^2}}\,\mathrm{d}t\right\} \tag{25}$$

$$f\left(x_A\right)=\sum_{n=1}^{N}\left\{P_{rob}\left(B_n\right)\frac{1}{\sigma_n\sqrt{2\pi}}e^{\frac{-(x_A-\mu_n)^2}{2\sigma_n^2}}\right\} \tag{26}$$

Where $F(x_A|B_n)$ is the CDF that the state variable x is less than x_A when the wind power output power is in the n^{th} state; μ_n and σ_n are respectively the expected value and standard deviation of the state variable x obtained by calculating the PPF, considering the random changes of the bus loads when the wind power in the grid is in the n^{th} state.

The relationship between the cumulant and origin moment is shown in Eq. (27). The properties of the TPF can be satisfied based on the origin moment from Eq. (27). The origin moment of each state variable considering all combined states is shown in Eq. (28) [39]. Then, the inverse transformation of Eq. (27) is used to obtain the final second-order cumulant of the state variable. The center moments of other orders can also be calculated using the above method.

$$\begin{cases}\alpha_1=\kappa_1\\ \alpha_2=\kappa_1+\kappa_1^2\end{cases}\ \text{or}\ \begin{cases}\kappa_1=\alpha_1\\ \kappa_2=\alpha_2-\alpha_1^2\end{cases} \tag{27}$$

$$\begin{cases}\alpha_1=\sum_{n=1}^{N}\alpha_{1,n}P_{rob}\left(B_n\right)=\sum_{n=1}^{N}\kappa_{1,n}P_{rob}\left(B_n\right)\\ \alpha_2=\sum_{n=1}^{N}\alpha_{2,n}P_{rob}\left(B_n\right)=\sum_{n=1}^{N}\left(\kappa_{2,n}+\kappa_{1,n}^2\right)P_{rob}\left(B_n\right)\end{cases} \tag{28}$$

Where α_1 represents the first-order origin moment; $\alpha_{1,n}$ represents the origin moment in the n^{th} output state of wind power generation; κ is the symbol index has the same meaning as the cumulant of the state variable.

3.5 Evaluation indicators

3.5.1 Probability of voltage deviation

Voltage deviation probability measures how likely bus voltages are to exceed safe limits during grid operation. This probability depends on grid conditions, load variations, generation uncertainties, and weather effects. As the deviation increases, the risk of voltage deviation also increases. Such deviations may damage equipment, reduce power quality, or cause system failures. Equation (29) provides the method to calculate this probability [40]:

$$F\left(V_i\right)=\begin{cases}\int_{-\infty}^{U_{\min}}f\left(V_i\right)\mathrm{d}V, & V_i<V_{\min}\\ 0, & V_{\min}<V_i<V_{\max}\\ \int_{U_{\max}}^{+\infty}f\left(V_i\right)\mathrm{d}V, & V_i>V_{\max}\end{cases}, \tag{29}$$

where $f(V_i)$ is the voltage probability density function of the bus i; $F(V_i)$ is the risk value for voltage deviation; V_i is the per unit value of bus voltage; i-bus number; $V_{\max}$ and $V_{\min}$ are the upper and lower limits of the allowable range of bus voltage, respectively.

3.5.2 Severity of voltage deviation

Different forms of utility functions reflect decision-maker's attitudes toward risk perception, which are generally divided into three types: risk aversion, risk neutrality, and risk preference. The functional characteristics of the risk preference utility function are shown in Eq. (30) [41]:

$$M\left(\theta\right)=\frac{e^{\gamma\theta}-1}{e-1}, \tag{30}$$

where θ is the severity risk indicator: $\gamma \geq 0$ is generally taken as $\gamma = 1$. The severity function for voltage exceeding a given threshold is generally $M'(\theta) > 0$, $M''(\theta) > 0$.

The distribution network needs to have safe and reliable power supply capabilities. As the distribution network directly faces the user terminal, it must ensure qualified power quality, that is, $M'(\theta) > 0$. At the same time, an increase in voltage fluctuation range will inevitably cause voltage to exceed the limit, that is, $M''(\theta) > 0$. Therefore, this paper adopts a risk preference utility function to characterize the severity model of events, which reflects the network's ability to withstand voltage exceeding limits and is closer to the actual situation of the distribution system [31]. Its utility function can be expressed as

$$M(\theta) = 0.582\left(e^{\theta} - 1\right). \tag{31}$$

Voltage deviation shows how far distribution network bus voltages move from normal levels, indicating collapse risk. Larger deviations cause more serious voltage problems. This paper defines the severity risk index θ as shown in Eq. (32):

$$\theta = \begin{cases} \dfrac{V_{\min} - V_i}{V_B - V_i}, & V_i < V_{\min} \\ 0, & V_{\min} < V_i < V_{\max} \\ \dfrac{V_i - V_{\max}}{V_i - V_B}, & V_i > V_{\max} \end{cases}, \tag{32}$$

where $V_{\max}$ and $V_{\min}$ are the upper and lower limits of the allowable range of bus voltage, respectively, and V_B is the reference voltage.

3.5.3 Comprehensive evaluation index for voltage deviation risk

Taking into account the probability and severity of voltage deviation, the comprehensive risk index R_s for voltage exceeding in the distribution network is shown in Eq. (33) [42]:

$$R_s = \sum_{i=1}^{n} R_i = \int_{-\infty}^{V_{\min}} f(V_i) \cdot M(\theta) \mathrm{d}V_i + \int_{V_{\max}}^{+\infty} f(V_i) \cdot M(\theta) \mathrm{d}V_i, \tag{33}$$

where R_i represents the comprehensive risk index of voltage deviation of the system bus i; n is the total number of buses.

3.6 Voltage deviation risk assessment calculation process

Fig. 2 shows the PPF calculation based on TPF considering correlation for voltage deviation risk assessment. The specific steps are as follows:

1. According to Eqs. (5) and (6), the probability model of the load is developed and the second-order semi-variables of the load are obtained.
2. The rated power of wind power is segmented step-by-step.
3. According to Eqs. (20) and (21), N times deterministic power flow is calculated.
4. Wind power is obtained by utilizing the relationship of wind speed in Eq. (3) and the Nataf transform for the correlation of wind speed for the wind speed.
5. The wind power is matched with the segmented power to obtain the probability of each subsection.
6. The PDF of the output random variable can be obtained from Eqs. (25) and (26).
7. Calculate the voltage deviation probability and severity. Then determine the comprehensive overvoltage risk index using Eq. (33).
8. The comprehensive risk of voltage deviation in distribution networks under different operating conditions is evaluated.

4 Results and discussion

4.1 Test system and input data

The IEEE-33 bus simulation system was established based on the MATLAB platform to demonstrate the correctness and effectiveness of the proposed TPF method in this paper [21]. Fig. 3 depicts the topology of the IEEE-33 bus system, highlighting the positions of critical buses and wind turbine connections. The original load data uses the sample mean as its baseline value, with a variation coefficient of 0.1. Buses 18 and 33 are electrically distant from generators, making them weak voltage points in the system. In order to mitigate voltage drops at these weak buses, wind turbines with capacities of 600 kW and 400 kW were connected to buses 18 and 33, respectively [22]. Wind turbines operate at a constant power factor and receive reactive power from the grid.

According to Eqs. (1) and (2) in Section 2, the Weibull distribution parameters are fitted based on historical measured wind speed data. The scale and shape parameters of wind speed can be obtained as λ = 10.7 m/s and k = 2.7, respectively. The cut-in wind speed rated wind speed, and excised wind speed of wind turbine are respectively 3 m/s, 18 m/s and 25 m/s [17]. According to the relationship between the output active power of wind turbines and wind speed in Eq. (3), the active power of wind turbines follows a non-normal distribution. This paper proposes the TPF method for PPF calculation. The 10^4 MCS results serve as the benchmark. The TPF calculation results were compared with the 2PEM calculation results to verify the accuracy and effectiveness of the method proposed in this paper.

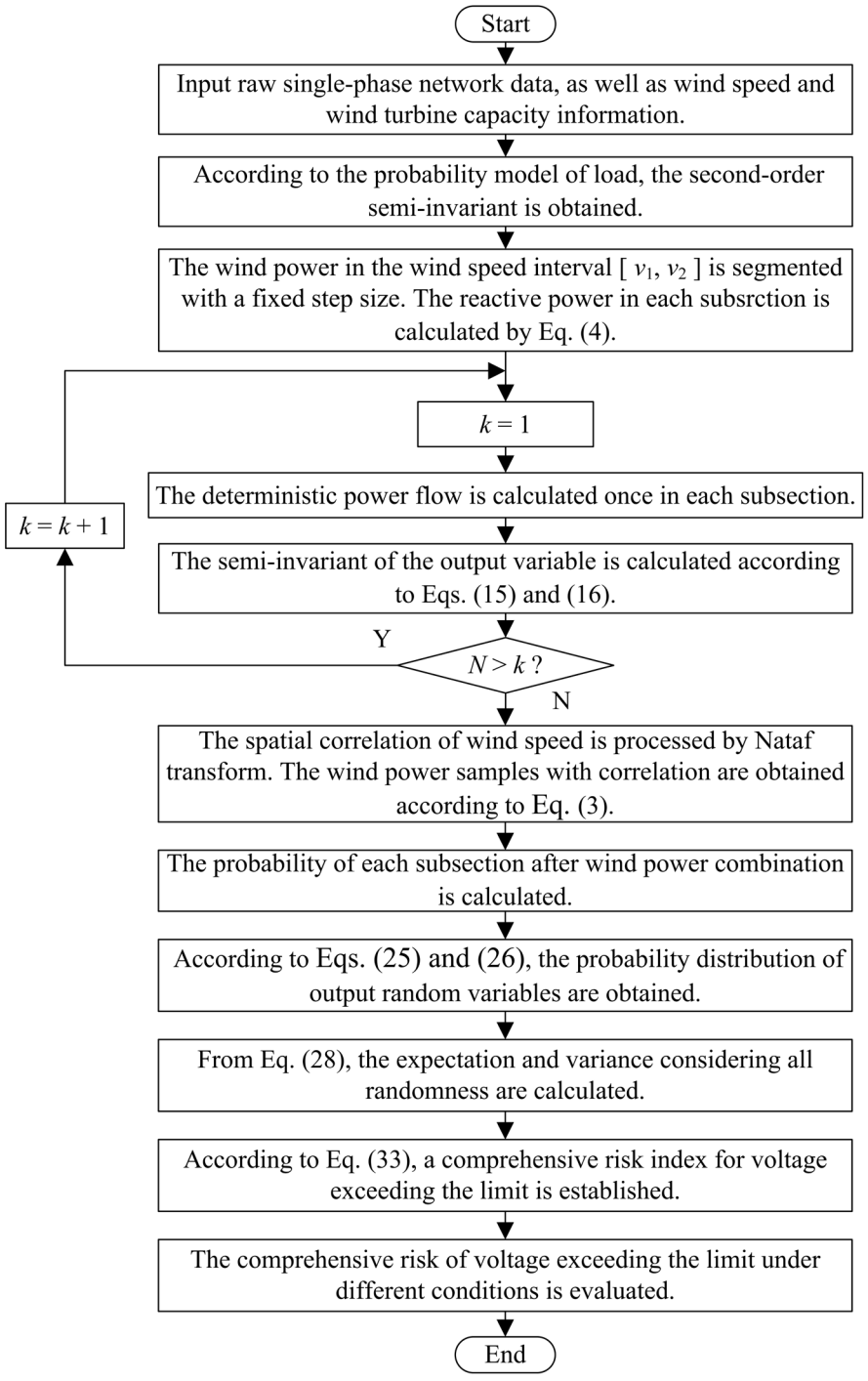

Fig. 2 Flowchart of PPF calculation using the TPF method considering the correlation

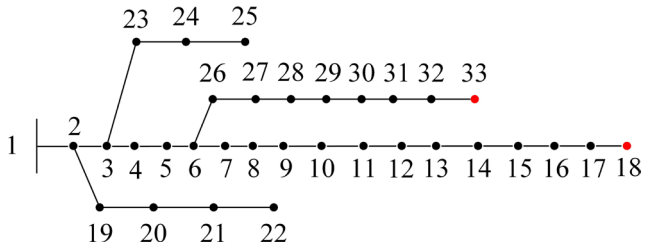

Fig. 3 Topology diagram of IEEE-33 bus system

4.2 Results of PPF

To visually demonstrate the accuracy of the proposed TPF method, the MCS method was used as a benchmark to compare the TPF and 2PEM methods. The 18 and 33 buses connected to the wind turbine, as well as the 22 and 25 buses that are far away from the wind turbine connection bus, are analyzed as examples. As presented in Fig. 4, shows that the

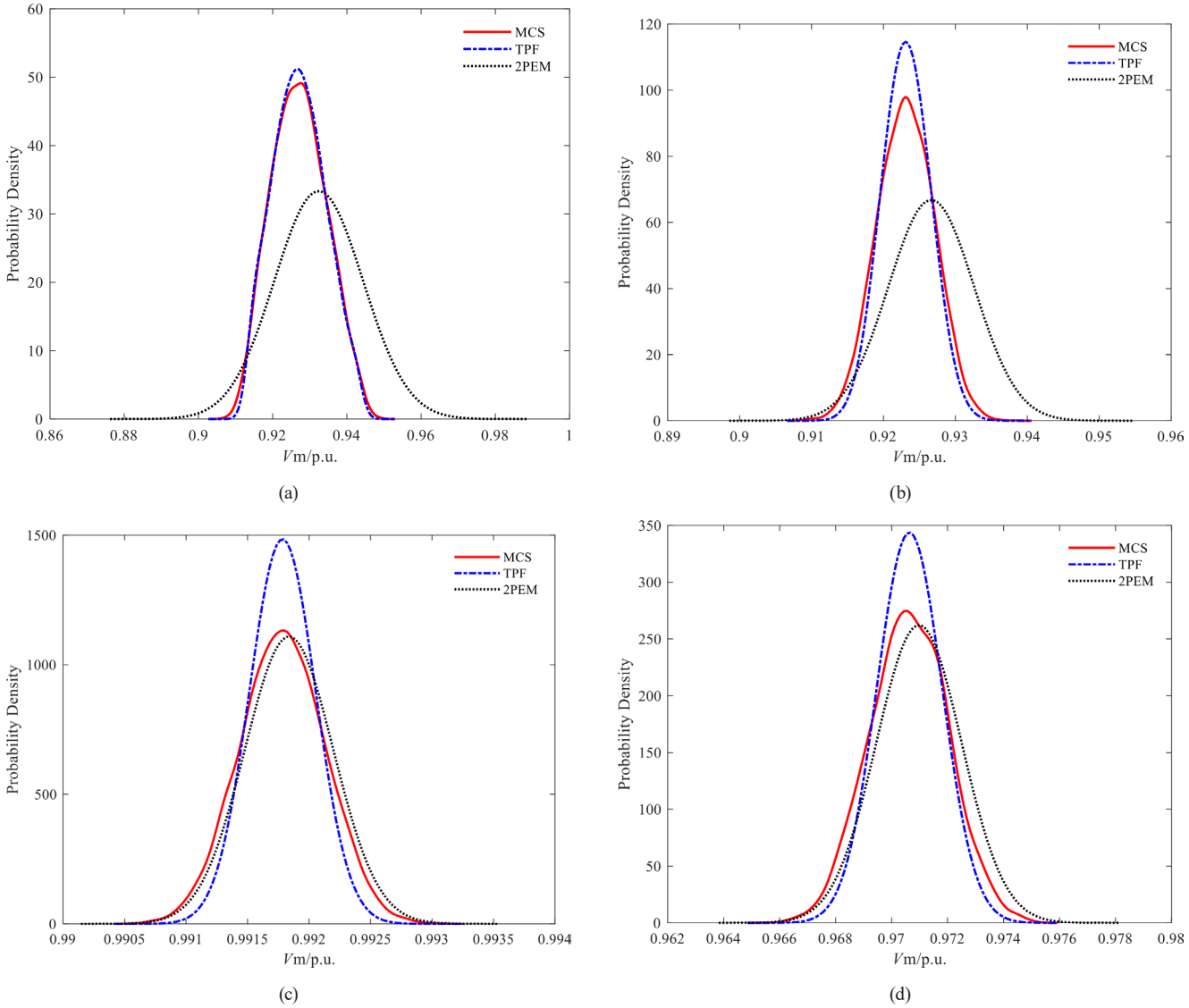

Fig. 4 Voltage probability density obtained by different calculation methods: (a) Bus No. 18, (b) Bus No. 33, (c) Bus No. 22, (d) Bus No. 25

voltage probability density curves vary depending on the proximity of the bus to the wind turbine and the distribution characteristics of the input random variables. At buses 18 and 33, where the wind turbine is directly connected, the results from the TPF method closely match those from the MCS method, demonstrating the method's high accuracy. In contrast, for buses 22 and 25, which are farther from the turbine, the input random variables tend to follow the normal distribution more closely, leading to a better performance of the 2PEM method compared to TPF. This detailed comparison underscores the capability of the TPF method in handling non-normal random variables more effectively.

4.3 The analysis of calculation error

To quantitatively compare the overall performance of the TPF method proposed in this paper, Average errors $\bar{\xi}_{\mu}$ and $\bar{\xi}_{\sigma}$ are defined for each output random variable, as shown in Eqs. (34) and (35), respectively. The smaller the $\bar{\xi}_{\mu}$ and $\bar{\xi}_{\sigma}$ indicators, the better the performance of the calculation method. The specific results of the error results are shown in Table 2, which have variable indicators such as voltage amplitude (V_m), voltage phase angle (V_a), active power and reactive power (P_{ij} and Q_{ij}).

$$\bar{\xi}_{\mu} = \frac{\sum_{i=1}^{N_r} \left| \mu_{\mathrm{MCS}} - \mu_0 \right|}{N_r} \times 100[\%] \tag{34}$$

$$\bar{\xi}_{\sigma} = \frac{\sum_{i=1}^{N_r} \left| \sigma_{\mathrm{MCS}} - \sigma_0 \right|}{N_r} \times 100[\%] \tag{35}$$

Where μ_{MCS} and σ_{MCS} represents the average and standard deviation of each output random variable calculated by the MCS method, while μ_0 and σ_0 represents the average and

Table 2 Comparison of calculation accuracy under different segmentation step sizes

Cases	k = 20 kW				k = 25 kW				k = 40 kW			
	TPF (%)		2PEM (%)		TPF (%)		2PEM (%)		TPF (%)		2PEM (%)	
Results	ξ_μ	ξ_σ	ξ_μ	ξ_σ	ξ_μ	ξ_σ	ξ_μ	ξ_σ	ξ_μ	ξ_σ	ξ_μ	ξ_σ
V_m	0.0020	0.0210	0.2017	0.1311	0.0018	0.0210	0.2017	0.1311	0.0022	0.0208	0.2017	0.1311
V_a	0.0002	0.0124	0.2635	0.1144	0.0005	0.0122	0.2635	0.1144	0.0001	0.0127	0.2635	0.1144
P_{ij}	0.0035	0.0053	0.0302	0.0203	0.0027	0.0053	0.0302	0.0203	0.0041	0.0042	0.0302	0.0203
Q_{ij}	0.0023	0.0021	0.6863	0.0557	0.0027	0.0022	0.6863	0.0557	0.0020	0.0016	0.6863	0.0557

standard deviation of the output random variables calculated by the other two methods except MCS; N_r is the number of random variables.

4.4 Comparison of calculation time

In the IEEE-33 bus system, the TPF method's computation time varies with wind power segmentation step sizes. As in Section 4.3, the calculation speed of different methods is compared under three different step sizes. Table 3 compares computation times for MCS, TPF, and 2PEM methods using these step sizes.

Table 3 shows TPF's efficiency improvements over MCS: 68.36% faster at 20 kW, 80.40% at 25 kW, and 88.77% at 40 kW step sizes. Larger step sizes significantly reduce TPF's computation time, but require balancing speed with accuracy. While 2PEM shows minimal computation time variation, TPF offers greater advantages when considering both computational accuracy and speed.

In summary, the proposed TPF method demonstrates three key advantages when using optimal step sizes:

1. It computes faster than both MCS and 2PEM,
2. handles non-normal distributions more effectively,
3. maintains superior calculation accuracy.

These combined benefits make TPF particularly suitable for probabilistic power flow analysis and voltage deviation risk assessment applications.

4.5 Average and standard deviation with different levels of correlation

Fig. 5 shows the bus voltage average and standard deviation. Fig. 5 (a) reveals that wind power correlation levels have minimal impact on average voltage amplitudes.

Table 3 Comparison of calculation time

k (kW)	Calculation time (s)			Improved efficiency of TPF (%)
	MCS	TPF	2PEM	
20	33.8750	10.7188	7.2813	68.3579
25	33.5625	6.5781	7.4531	80.4004
40	34.7813	3.9063	7.6094	88.7691

However, Fig. 5 (b) demonstrates that voltage standard deviation increases with higher wind speed correlations. Stronger correlations make different wind turbine's outputs more similar yet more volatile. Buses closer to wind turbines experience greater standard deviation changes.

4.6 Probability density of voltage amplitudes with different correlations

Fig. 6 displays the voltage probability density for buses 18 and 33. As wind power correlation increases from 0.1 to 0.9, the probability density curve shifts from "thin and tall" to "short and fat". This change indicates a wider voltage fluctuation range under higher correlations. Consequently, stronger correlations raise the risk of voltage deviations.

4.7 Probability assessment of voltage deviation risk

4.7.1 Probability assessment of voltage deviation risk when connecting different wind turbine capacities

Fig. 7 shows the voltage probability density curves for buses 18 and 33. As wind turbine capacity grows from 400 kW to 1600 kW, the curve shifts rightward, indicating higher average voltages. While wind power improves voltage levels, it also widens the fluctuation range, increasing grid uncertainty.

Fig. 8 shows the voltage probability density for buses 18 and 33. When connected wind turbine capacity reaches 4200 kW and 4800 kW, the voltage exceeds the upper limit. Fig. 8 demonstrates that higher wind turbine capacity reduces low-voltage probability but increases overvoltage risk.

Fig. 9 shows the voltage deviation risk at each bus for different wind turbine capacities (without wind speed correlation). As wind turbine capacity increases, the risk index decreases. Fig. 7 reveals that higher capacities (within a range) boost voltage and reduce lower-limit violations. Small capacities avoid upper-limit violations, but at 4200 kW (Fig. 8), upper-limit violations occur. Thus, risk initially decreases with capacity but rises for upper-limit violations. The 4200 kW case is theoretical; practical networks may not support it. Hence, this study uses 1600 kW as the maximum capacity.

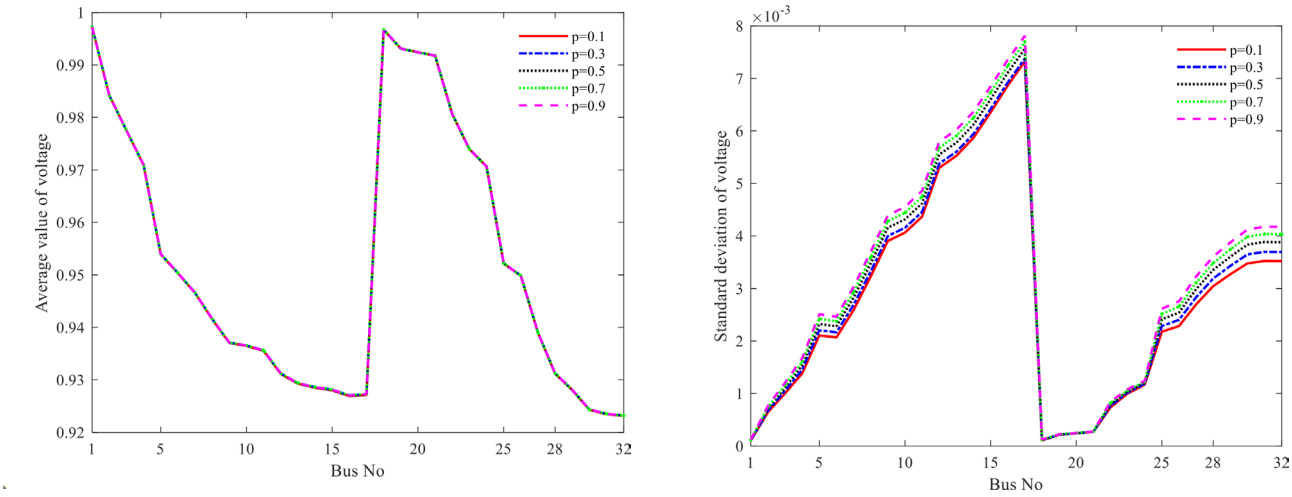

(a) (b)

Fig. 5 Average and standard deviation of voltage at different levels of correlation: (a) The average value of voltage, (b) Standard deviation of voltage

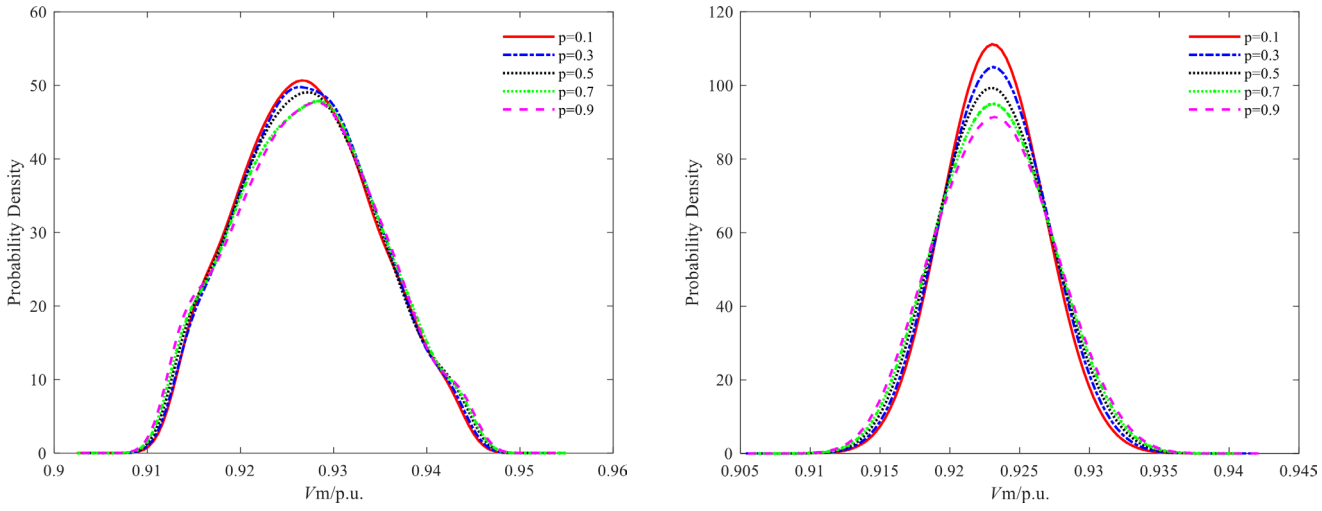

(a) (b)

Fig. 6 Voltage probability density curves at different levels of correlation: (a) Bus No. 18, (b) Bus No. 33

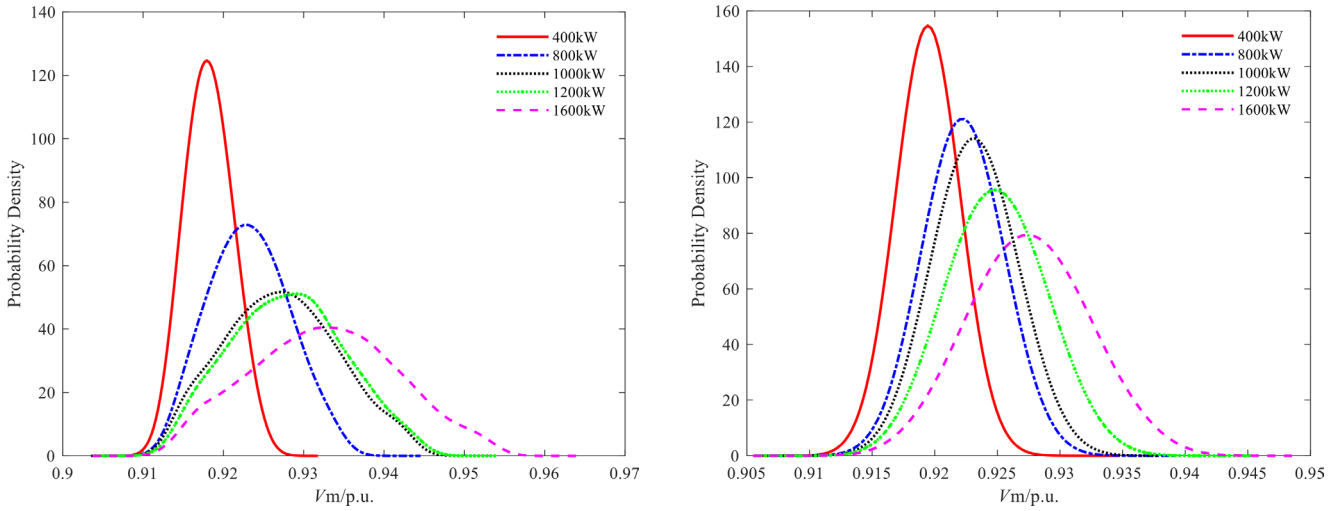

(a) (b)

Fig. 7 Voltage probability density curves under different access capacities: (a) Bus No. 18, (b) Bus No. 33

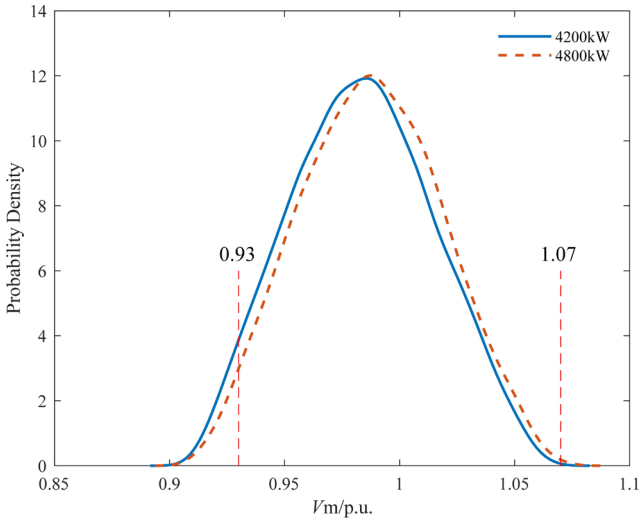

(a)

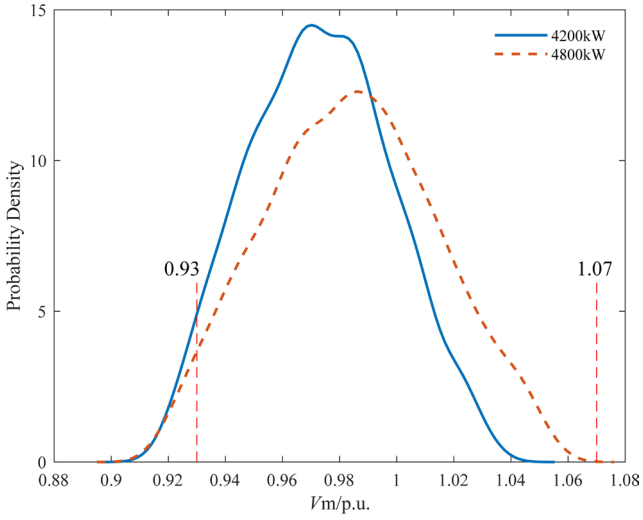

(b)

Fig. 8 Voltage probability density curves when connected to a large-capacity wind turbine: (a) Bus No. 18, (b) Bus No. 33

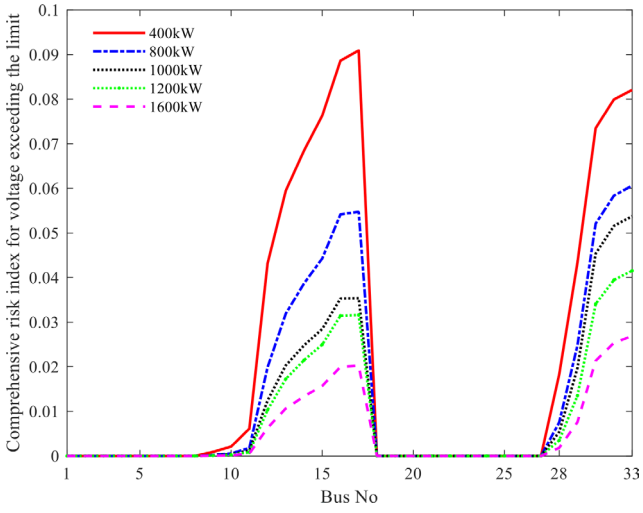

Fig. 9 Comprehensive risk of voltage deviation under different connected wind turbine capacities

Table 4 presents bus voltage indicators for different wind turbine capacities. As capacity increases from 400 kW to 1600 kW, three trends occur:

1. voltage deviation probability decreases,
2. utility function value declines, and
3. comprehensive risk index drops significantly from 0.7332 to 0.1699.

This 77% risk reduction greatly improves distribution network safety. These results match practical experience - within this capacity range, larger wind turbines effectively boost voltage and reduce lower-limit violation risks.

4.7.2 Probability assessment of voltage risk at different levels of correlation

Fig. 10 shows the voltage deviation risk index at 1600 kW wind capacity across different correlation levels. Higher correlation levels increase the risk index, especially at wind turbine connection buses. Stronger correlations make wind turbine outputs more consistent, disrupting distribution network operation. The impact grows stronger closer to the wind turbine buses.

Table 4 Voltage indicators under different connected wind turbine capacities

Voltage index	*P* (kW)				
	400	800	1000	1200	1600
Probability of exceeding the limit	0.3638	0.2972	0.2389	0.2097	0.1425
Utility function value	0.7811	0.5823	0.5258	0.4926	0.4361
Comprehensive risk indicators	0.7332	0.4496	0.3342	0.2704	0.1699

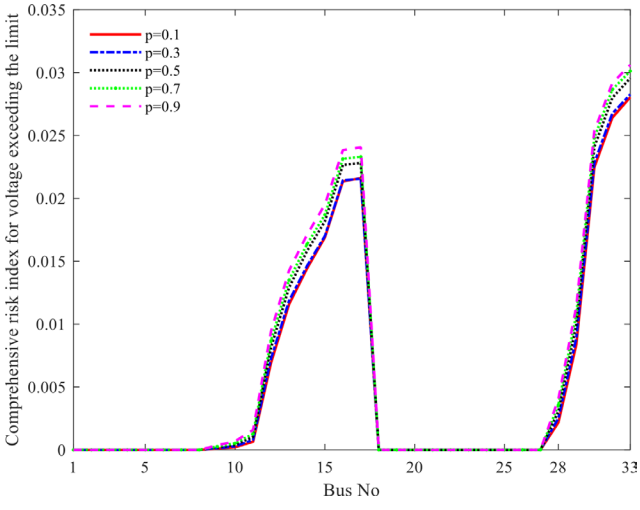

Fig. 10 Comprehensive risk indicators for voltage exceeding limits at different levels of correlation

Table 5 shows clear trends as wind power correlation increases from 0.1 to 0.9. The probability of voltage deviation rises steadily. Utility function values show consistent growth. The comprehensive risk index climbs from 0.1812 to 0.2114. This 16.7% increase signals higher operational risks for the distribution network. Stronger correlation creates tighter coupling between wind turbine outputs. This synchronization leads to network instability. Voltage deviation violations become more likely.

As shown above, the capacity and correlation level of wind turbines connected will affect the voltage risk of the distribution network. Within a certain range, the larger the capacity of the connected wind turbine, the lower the voltage risk of the distribution network. The higher the correlation level, the higher the voltage risk of the distribution network.

5 Conclusions

This paper proposes a probability assessment method for calculating voltage deviation risk using PPF based on TPF, taking into account the correlation of wind speed. Firstly, the Pearson correlation coefficient is used to characterize the correlation of wind speed. The Nataf transform is used to process the correlation of wind speed. Within the linear range of wind power, considering the calculation accuracy and speed of TPF, the output power of wind turbines is discretized with a fixed segmented step size. Secondly, this paper proposes a TPF method to solve PPF for distribution networks with wind turbines. The method obtains numerical characteristics and PDFs of the output random variables. Then, this work establishes a voltage deviation risk index. The index incorporates two factors: the probability of voltage deviation, and the severity of deviation. Finally, the accuracy and speed of the proposed method were verified in the IEEE-33 bus system. Obtain the following results:

Table 5 Voltage indicators at different correlation levels

Voltage index	Correlation level				
	0.1	0.3	0.5	0.7	0.9
Probability of exceeding the limit	0.1474	0.1459	0.1493	0.1495	0.1503
Utility function value	0.4532	0.4387	0.4630	0.4734	0.4509
Comprehensive risk indicators	0.1812	0.1842	0.1968	0.2037	0.2114

1. The implementation of segmented linearization for wind power output discretization enhances computational efficiency while maintaining required accuracy levels.
2. The correlation of wind power outputs shows negligible influence on the average voltage amplitude at system buses. However, stronger correlations lead to significantly higher standard deviations in bus voltage amplitude. Notably, buses electrically closer to wind power sites experience more pronounced voltage fluctuations.
3. The higher the correlation level, the higher the probability of voltage deviation, and the higher the comprehensive risk index of voltage deviation.
4. Within a certain range, increasing the capacity of connected wind turbines can elevate the bus voltage, thereby decreasing the probability of voltage falling below the lower limit and mitigating the overall voltage deviation risk. However, when the wind power capacity exceeds a certain threshold, the bus voltage may rise beyond the upper limit, leading to an increased risk of overvoltage.

The TPF method proposed in this paper is suitable for analyzing and calculating the safe operation and planning scheduling of high-proportion wind power integration into distribution networks considering the uncertainty and has certain feasibility. Building on the current research, future work will investigate hybrid PV-wind distribution networks. Specifically, the proposed method will be applied to investigate how photovoltaic (PV) and wind power interactions influence grid operation. One limitation of the proposed method is its inability to automatically select segmentation step sizes. Automated selection of segmentation step sizes would better balance computational accuracy and speed.

Acknowledgement

The authors would like to thank the support provided by Hainan Power Grid Co., Ltd., as well as the staff who have provided their valuable assistance to this paper.

Funding statement

This work was supported by China Southern Power Grid Co., Ltd. Technology Project (Project Number: 070000KC23100011).

References

[1] Li, C., Li, Y., Xia, S., Wang, P., Ge, Q., Song, L., Li, Y. "A two-stage adaptive-robust optimization model for active distribution network with high penetration wind power generation", IET Renewable Power Generation, 18(7), pp. 1204–1217, 2024. https://doi.org/10.1049/rpg2.12836

[2] National Energy Administration "国家能源局" (National Energy Administration), [online] Available at: https://www.nea.gov.cn/ [Accessed: 11 April 2025] (in Chinese)

[3] International Center for Science & Technology Innovation "China's wind and solar power utilization rates remain above 95% in 2024", 2024. [online] Available at: https://en.ncsti.gov.cn/Latest/news/202412/t20241216_189555.html [Accessed: 11 April 2025]

[4] Jia, F., Fu, Y. "The Gradual Follow-up Essence of Wind Power Tracking and the Non-communication Centralized Power Conversion Principle for Wind Turbine Cluster", Proceedings of the CSEE, 43(15), pp. 5877–5890, 2023. https://doi.org/10.13334/j.0258-8013.pcsee.220420

[5] Abed, W. N. A.-D. "Solving probabilistic optimal power flow with renewable energy sources in distribution networks using fire hawk optimizer", E-Prime - Advances in Electrical Engineering, Electronics and Energy, 6, 100370, 2023. https://doi.org/10.1016/j.prime.2023.100370

[6] Ma, Z., Cao, F. "Optimization of Active Distribution Network Operation with SOP Considering Reverse Power Flow", Applied Sciences, 14(24), 11797, 2024. https://doi.org/10.3390/app142411797

[7] Xie, Y., Cai, S., Qin, X., Wu, H., Zhou, Q., Zhu, D., Wu, Q. "Coordinated day-ahead reactive power dispatch in distribution system considering spatial-temporal correlation of wind power", Sustainable Energy, Grids and Networks, 41, 101591, 2025. https://doi.org/10.1016/j.segan.2024.101591

[8] Zhang, Y., Gao, Y., Yang, S., Yue, X. "Response analysis of asymmetric monostable energy harvester with an uncertain parameter", International Journal of Non-Linear Mechanics, 163, 104752, 2024. https://doi.org/10.1016/j.ijnonlinmec.2024.104752

[9] Wang, T., Wang, S., Ma, S., Guo, J., Zhou, X. "An extended continuation power flow method for static voltage stability assessment of renewable power generation-penetrated power systems", IEEE Transactions on Circuits and Systems II: Express Briefs, 71(2), pp. 892–896, 2022. https://doi.org/10.1109/TCSII.2022.3209335

[10] Amjady, N., Ansari, M. R. "Small disturbance voltage stability assessment of power systems by modal analysis and dynamic simulation", Energy Conversion and Management, 49(10), pp. 2629–2641, 2008. https://doi.org/10.1016/j.enconman.2008.04.010

[11] Liao, X., Zhang, Y., Li, Z., Wei, H., Ding, H. "Probabilistic interval power flow calculation method for distribution networks considering the correlation of distributed wind power output", International Journal of Electrical Power & Energy Systems, 157, 109827, 2024. https://doi.org/10.1016/j.ijepes.2024.109827

[12] Koirala, A., Van Acker, T., D'hulst, R., Van Hertem, D. "Hosting capacity of photovoltaic systems in low voltage distribution systems: A benchmark of deterministic and stochastic approaches", Renewable and Sustainable Energy Reviews, 155, 111899, 2022. https://doi.org/10.1016/j.rser.2021.111899

[13] Lopez-Ramirez, I., Rodriguez-Seco, J. E., Zamora, I. "Assessment on power systems non-deterministic state estimation algorithms", Electric Power Systems Research, 214, 108880, 2023. https://doi.org/10.1016/j.epsr.2022.108880

[14] Wang, D., Yang, M., Zhang, W., Ma, C., Su, X. "Short-term power prediction method of wind farm cluster based on deep spatiotemporal correlation mining", Applied Energy, 380, 125102, 2025. https://doi.org/10.1016/j.apenergy.2024.125102

[15] Che, Y., Lü, X., Wang, X. "考虑相关性的牵引负荷功率对电网影响概率分析" (Probabilistic analysis of impact of traction load power on power grid considering correlation), Proceedings of the CSEE, 42(09), pp. 3250–3261, 2022. (in Chienese) https://doi.org/10.13334/j.0258-8013.pcsee.210280

[16] Kan, R., Xu, Y., Li, Z., Lu, M. "Calculation of probabilistic harmonic power flow based on improved three-point estimation method and maximum entropy as distributed generators access to distribution network", Electric Power Systems Research, 230, 110197, 2024. https://doi.org/10.1016/j.epsr.2024.110197

[17] Martins, A. S. C., de Araujo, L. R., Penido, D. R. R. "An active multiphase probabilistic power flow based on a clustering approach", Electric Power Systems Research, 230, 110264, 2024. https://doi.org/10.1016/j.epsr.2024.110264

[18] Sobrinho Campolina Martins, A., Ramos de Araujo, L., Rosana Ribeiro Penido, D. "K-Medoids clustering applications for high-dimensionality multiphase probabilistic power flow", International Journal of Electrical Power & Energy Systems, 157, 109861, 2024. https://doi.org/10.1016/j.ijepes.2024.109861

[19] Singh, V., Moger, T., Jena, D. "Maximum entropy based probabilistic load flow for assessing input uncertainties and line outages in wind-integrated power systems", Electric Power Systems Research, 244, 111528, 2025. https://doi.org/10.1016/j.epsr.2025.111528

[20] Singh, V., Moger, T., Jena, D. "Probabilistic load flow approach combining cumulant method and K-means clustering to handle large fluctuations of stochastic variables", IEEE Transactions on Industry Applications, 59(3), pp. 2832–2841, 2023. https://doi.org/10.1109/TIA.2023.3239558

[21] Ma, Z., Zhang, Q., Wang, Z. "Safe and stable secondary voltage control of microgrids based on explicit neural networks", IEEE Transactions on Smart Grid, 14(5), pp. 3375–3387, 2023. https://doi.org/10.1109/TSG.2023.3239548

[22] Yu, J., Li, Q., Du, Y., Wang, R., Li, R., Guo, D. "Voltage over-limit risk assessment of wind power and photovoltaic access distribution system based on day-night segmentation and Gaussian mixture model", Energy Reports, 12, pp. 2812–2823, 2024. https://doi.org/10.1016/j.egyr.2024.08.079

[23] Nejadfard-jahromi, S., Mohammadi, M., Kargarian, A. "Nonparametric preventive/corrective voltage stability enhancement of active distribution systems with integrated electric vehicles charging facilities", International Journal of Electrical Power & Energy Systems, 129, 106813, 2021. https://doi.org/10.1016/j.ijepes.2021.106813

[24] Canudo, J., Sevillano, P., Iranzo, A., Kwik, S., Preciado-Garbayo, J., Subias, J. (2024) "Simultaneous Structural Monitoring over Optical Ground Wire and Optical Phase Conductor via Chirped-Pulse Phase-Sensitive Optical Time-Domain Reflectometry", Sensors, 24(22), 7388, 2024. https://doi.org/10.3390/s24227388

[25] Çekyay, B., Frenk, J. B. G., Javadi, S. "On computing the multivariate Poisson probability distribution", Methodology and Computing in Applied Probability, 25(3), 70, 2023. https://doi.org/10.1007/S11009-023-10036-Z

[26] Al-Din Abed, W. N. "A novel improved harbor seal whiskers algorithm for solving hybrid dynamic economic environmental dispatch considering uncertainty of renewable energy generation", E-Prime - Advances in Electrical Engineering, Electronics and Energy, 9, 100685, 2024. https://doi.org/10.1016/j.prime.2024.100685

[27] Su, C., Liu, C., Li, Z., Zhou, M. "基于贝叶斯理论的考虑多维风速之间相关性的概率潮流计算" (Bayesian theory based calculation of probabilistic power flow considering correlation between multi-dimensional wind speed), Automation of Electric Power Systems, 45(3), pp. 157–165, 2021. (in Chinese) https://doi.org/10.7500/AEPS20200116004

[28] Al-Din Abed, W. N., Imran, O. A., Abdullah, A. N. "Sensored speed control of brushless DC motor based salp swarm algorithm", International Journal of Electrical and Computer Engineering (IJECE), 12(5), pp. 4832–4840, 2022. https://doi.org/10.11591/ijece.v12i5.pp4832-4840

[29] Al-Din Abed, W. N., Imran, O. A., Fatah, I. S. "Automatic generation control based whale optimization algorithm", International Journal of Electrical and Computer Engineering (IJECE), 9(6), pp. 4516–4523, 2019. https://doi.org/10.11591/ijece.v9i6.pp4516-4523

[30] Abed, W. N. A.-D., Saleh, A. H., Hameed, A. S. "Speed Control of PMDCM Based GA and DS Techniques", International Journal of Power Electronics and Drive Systems (IJPEDS), 9(4), pp. 1467–1475, 2018. https://doi.org/10.11591/ijpeds.v9.i4.pp1467-1475

[31] Chen, H., El-Refaie, A. M., Zuo, Y., Cai, S., Tang, J., Liu. Y., Lee, C. H. T. "A permanent magnet brushless doubly fed electric machine for variable-speed constant-frequency wind turbines", IEEE Transactions on Industrial Electronics, 70(7), pp. 6663–6674, 2023. https://doi.org/10.1109/TIE.2022.3201306

[32] Sharma, R., Shikhola, T., Kohli, J. K. "Modified fuzzy Q-learning based wind speed prediction", Journal of Wind Engineering and Industrial Aerodynamics, 206, 104361, 2020. https://doi.org/10.1016/j.jweia.2020.104361

[33] dos Santos., A. S., Borges, C. L. T., Barboza, R. R. "A methodology to correlate river inflows in state sampling Monte Carlo simulation", Electric Power Systems Research, 236, 110926, 2024. https://doi.org/10.1016/j.epsr.2024.110926

[34] Pikuliński, M., Malczyk, P., Aarts, R. "Data-driven inverse dynamics modeling using neural-networks and regression-based techniques", Multibody System Dynamics, 63(3), pp. 341–366, 2025. https://doi.org/10.1007/s11044-024-10024-2

[35] Tan, B., Zhao, J., Chen, Y. "Scalable Risk Assessment of Rare Events in Power Systems with Uncertain Wind Generation and Loads", IEEE Transactions on Power Systems, 40(2), pp. 1374–1388, 2025. https://doi.org/10.1109/TPWRS.2024.3435490

[36] Yang, Y., Yang, Z., Yu, J., Zhang, B., Zhang, Y., Yu, H. "Fast Calculation of Probabilistic Power Flow: A Model-Based Deep Learning Approach", IEEE Transactions on Smart Grid, 11(3), pp. 2235–2244, 2020. https://doi.org/10.1109/TSG.2019.2950115

[37] Gao, Y., Wang, C. "级数展开法拟合概率潮流分布函数的局限及改进" (Limitation analysis and improvement for series expansion methods to fit the distribution function of probabilistic power flow), Proceedings of the CSEE, 41(17), pp. 5900–5911, 2021. (in Chinese) https://doi.org/10.13334/j.0258-8013.pcsee.201479

[38] Sun, F., Wu, N., Li, Y. "A Dual-Prior Conditional Probability Diffusion Model for Seismic Data Resolution Enhancement", IEEE Transactions on Geoscience and Remote Sensing, 63, 5909616, 2025. https://doi.org/10.1109/TGRS.2025.3556448

[39] Luo, X., Tang, T., Yin, J., Liu, H. "A robust MPC approach with controller tuning for close following operation of virtually coupled train set", Transportation Research Part C: Emerging Technologies, 151, 104116, 2023. https://doi.org/10.1016/j.trc.2023.104116

[40] Abbas, A. S., El-Ela, A. A. A., El-Sehiemy, R. A., Fetyan, K. K. "Assessment and Enhancement of Uncertain Renewable Energy Hosting Capacity With/out Voltage Control Devices in Distribution Grids", IEEE Systems Journal, 17(2), pp. 1986–1994, 2023. https://doi.org/10.1109/JSYST.2022.3180779

[41] Shen, Y., Wu, Y., Zhang, D., Liang, Y., Yin, D., Wang, L., Wang, L., Cao, J., Cheng, Y. "Stabilization of high-voltage layered oxide cathode by utilizing residual lithium to form NASICON-type nanoscale functional coating", Nano Research, 16(4), pp. 5973–5982, 2023. https://doi.org/10.1007/s12274-022-5298-y

[42] Deng, J., Lin, L., Zhang, Y., Ma, Y. "A Collaborative Planning Method for the Source and Grid in a Distribution System That Considers Risk Measurement", Energies, 16(15), 5648, 2023. https://doi.org/10.3390/en16155648